Available online at www.sciencedirect.com

ScienceDirect

International Journal of Solids and Structures 45 (2008) 2818–2835

INTERNATIONAL JOURNAL OF SOLIDS AND STRUCTURES

www.elsevier.com/locate/ijsolstr

A computational study on the instrumented sharp indentations with dual indenters

Minh-Quy Le *

Department of Mechanics of Materials & Structures, Faculty of Mechanical Engineering, Hanoi University of Technology, Dai Co Viet Road, Hanoi, Viet Nam

Received 16 July 2007; received in revised form 5 November 2007
Available online 13 January 2008

Abstract

Finite element analysis was performed to investigate the indentation response of elasto-plastic solids for conical indenters of half included angles of 60° and 70.3°. The interdependence indentation parameters resulting from a single indentation load–depth curve is considered. Regarding dimensional analysis, several dimensionless relationships are constructed as functions of the reduced elastic modulus-loading curvature ratio E^*/C and the strain hardening exponent n. Further, the duality between corresponding parameters with dual indenters is explored. Finally, a new method based on dual indenters is proposed to extract the strain hardening exponent and the reduced elastic modulus of an indented material. The accuracy of this method is verified and discussed with experimental data from the literature and representative materials.

Keywords: Instrumented indentation; Finite element analysis; Mechanical properties; Dual indenters

1. Introduction

Instrumented sharp indentation techniques are extensively developed to characterize various materials including metals, metallic alloys, ceramics, glasses, polymers, and coated materials, etc. (Doerner and Nix, 1986; Oliver and Pharr, 1992, 2004; Fischer-Cripps, 2004). Dimensional analysis is widely used to explore various aspects of indentation with the aid of finite element analysis (FEA) when necessary, see the recent review by Cheng and Cheng (2004). In this context, dimensionless functions have been formulated to relate indentation parameters with the indenter geometry and the indented material's mechanical properties such as elastic modulus E, yield strength Y and strain hardening exponent n. In the reverse analysis, such dimensionless functions have been used to extract the mechanical properties (Dao et al., 2001; Futakawa et al., 2001; DiCarlo et al., 2003; Bucaille et al., 2003; Chollacoop et al., 2003; Swaddiwudhipong et al., 2005; Ogasawara et al., 2005; Luo and Lin, 2007; Lan and Venkatesh, 2007).

* Tel./fax: +84 4 8680103.
E-mail address: quylm@mail.hut.edu.vn

0020-7683/$ - see front matter © 2008 Elsevier Ltd. All rights reserved.
doi:10.1016/j.ijsolstr.2007.12.022

The common method to construct dimensionless functions in instrumented indentation problems is based on the concept of representative strain, which was introduced by Atkins and Tabor (1965) and later extended by Dao et al. (2001) for a Vickers or a Berkovich pyramid or a conical indenter ($\theta = 70.3°$, see Fig. 1 for notations). Such dimensionless functions set up the relationships between characteristic parameters, C, S and h_r/h_m, of a P–h curve and the reduced elastic modulus E^*, the representative stress σ_r (which can be used to derive Y if n is known) and the strain hardening n. This concept was then developed by Bucaille et al. (2003) and Chollacoop et al. (2003) for dual or multiple indenters, and recently generalized by Ogasawara et al. (2005, 2006).

Direct use of E^*/Y and n as two key parameters to govern indentation parameters has been recently investigated by Swaddiwudhipong et al. (2005) and Luo and Lin (2007) for dual indenters with half included angles of 60° and 70.3°. Swaddiwudhipong et al. (2005) proposed a reverse analysis procedure based on the dimensionless functions C/Y and W_p/W_t. Luo and Lin (2007) constructed a set of dimensionless functions for characteristics of the loading and the 50% upper unloading curves. The authors supposed that the indentation force–depth response of an elastic–plastic material is a linear combination of the corresponding elastic and elastic–perfect plastic materials. An optimization method was then used in their reverse analysis.

Further, previous works have also focused on fundamental features in reverse analysis problems such as the sensitivity (Bucaille et al., 2003; Chollacoop et al., 2003; Cao and Lu, 2004; Swaddiwudhipong et al., 2005; Lan and Venkatesh, 2007) as well as the uniqueness of the reverse solution (Cheng and Cheng, 1999; Capehart and Cheng, 2003; Alkorta et al., 2005; Tho et al., 2005; Luo et al., 2006; Chen et al., 2007). Several authors have shown that the relationship between the mechanical properties (E^*, Y and n) and the resulting load–displacement curve is not one-to-one. Therefore, it is practically impossible to uniquely recover E^*, Y and n from the load–displacement curve of a single indenter (Cheng and Cheng, 1999; Capehart and Cheng, 2003; Alkorta et al., 2005; Tho et al., 2005; Luo et al., 2006). Furthermore, by using load–depth curves of a single indenter the non-unique solution is suffered from the interdependence of indentation parameters, since only two among four indentation parameters C, S, W_p/W_t, h_r/h_m are independent as discussed in Chen et al. (2007). Therefore, it is impossible to determine the mechanical properties (E^*, Y and n) by using load–depth curves of a single indenter.

Moreover, the unique solution in reverse analysis with dual indenters was recently investigated by Chen et al. (2007). The authors have demonstrated the possible existence of *mystical materials*, which experience almost identical P–h curves for different indenters of half included angles ranging from 60° to 80°. Hence, reverse analysis with dual or multiple indenters would fail since it cannot promise unique solution. They have also indicated that two mystical materials associated to dual indenters must exhibit fair difference in Young's modulus. This difference appears within 10% for all pairs of mystical materials, which have been specified in Chen et al. (2007). The range of mystical materials is rapidly reduced when increasing the difference between the apex angles of dual indenters. For specific dual indenters ($\theta_1 = 70.3°$, $\theta_2 = 80°$) and ($\theta_1 = 70.3°$, $\theta_2 = 63.14°$), only low strain hardening materials ($n \leqslant 0.2$) with $Y/E \approx 0.01$ may become mystical materials.

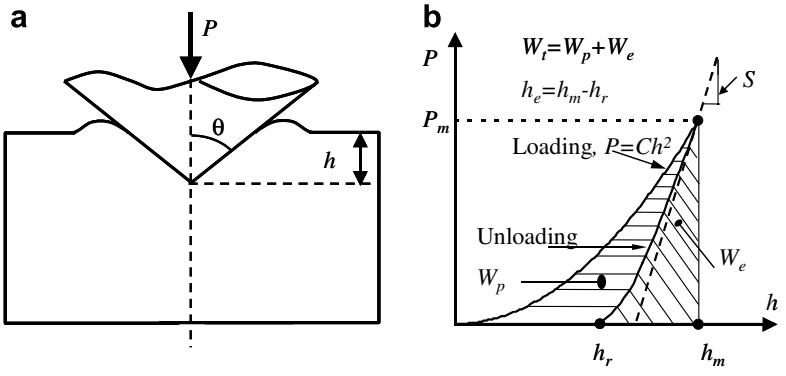

Fig. 1. Schematic representation of a conical indentation: (a) axisymmetric model of the indenter and specimen; (b) typical indentation load–depth curve.

For the common dual indenters ($\theta_1 = 70.3°$ and $\theta_2 = 60°$), very few useful mystical materials with low strain hardening has been found by Chen et al. (2007).

Overall, it may be seen from the literature that several issues should be investigated. Firstly, the interdependence of indentation parameters was shown. Thus, their systematic formulation is required. Secondly, dimensionless relationships in instrumented indentation problems are generally constructed as functions of the mechanical properties (E^*/Y or E^*/σ_r, and n), leading to non-linear and complex functional forms. Hence, the use of an indentation parameter instead of a mechanical property may be challenged in order to establish as simple as possible dimensionless functions as well as better understand the instrumented indentation phenomena. Further, in terms of dual indenters, the duality between corresponding parameters is rarely exploited even though multiple indenters have been used. Finally, a possible reverse procedure with the common dual indenters ($\theta_1 = 70.3°$, $\theta_2 = 60°$) may be considered for a wide range of materials. In case of mystical materials, it can allow to estimate accurately at least the Young's modulus since this mechanical property for a pair of mystical materials must be in fact fairly different.

The present work is aimed at addressing the above mentioned issues within the context of dimensional analysis and with the aid of FEA.

2. Theoretical backgrounds and finite element model

2.1. Theoretical backgrounds

Elastic–plastic behavior of many engineering solid materials can be modeled by a power law description. A simple elasto-plastic, true stress–true strain behavior is assumed to be:

$$\begin{aligned} \sigma &= E \cdot \varepsilon \quad (\sigma \leqslant Y) \\ \sigma &= K \cdot \varepsilon^n \quad (\sigma \geqslant Y) \end{aligned} \tag{1}$$

where E is the Young's modulus, K a strength coefficient, n the strain hardening exponent, Y the initial compressive uniaxial yield stress and ε_y the corresponding yield strain, such that

$$\sigma_y = E\varepsilon_y = K\varepsilon_y^n \tag{2}$$

Fig. 1b illustrates the typical indentation load–depth response of an elasto-plastic material to sharp indentation. Considering dimensional analysis and geometrical similarity of a conical/pyramid indenter, Cheng and Cheng (2004) have demonstrated that the indentation force P during loading is proportional to the square of the indentation depth h:

$$P = Ch^2 \tag{3}$$

Here, C is the loading curvature which is a measure of the resistance of the material to indentation. The form of P–h unloading curve has been approximated by the following power law relation (Oliver and Pharr, 1992):

$$P_u = A(h - h_r)^m \tag{4}$$

For a given conical/pyramid indenter, the indentation force P during loading can be expressed as (Dao et al., 2001; Cheng and Cheng, 2004):

$$P = P(h, E, v, E_i, v_i, Y, n) \tag{5}$$

where E and v, and E_i and v_i are the elastic modulus and Poisson's ratio of the indented material and the indenter, respectively.

It is remarked here that the reduced elastic modulus of two contacting bodies is commonly used when these bodies are capable of being represented as a half-space (Johnson, 1985). In the present study, the cone angle is relatively tight. Under elastic conditions, contact pressure distributions obtained by the analytical solution (Johnson, 1985) and FEA would become significantly different as the indenter apex angle is reduced (Lin et al., 2000). However, it can be checked that deviation in other indentation parameters such as the loading curvature C from two solutions is less sensitive to indenter apex angle. Thus, the indenter's elasticity effect is assumed to be considered in the analysis by using the reduced modulus as follows:

$$E^* = \left(\frac{1-\nu^2}{E} + \frac{1-\nu_i^2}{E_i}\right)^{-1} \tag{6}$$

Hence, Eq. (5) becomes:

$$P = P(h, E^*, Y, n) \tag{7}$$

Applying the Π-theorem in dimensional analysis, Eq. (7) can be written under the following form:

$$P = E^* h^2 f_1\left(\frac{Y}{E^*}, n\right) \tag{8}$$

Combining Eqs. (3) and (8), the reduced elastic modulus-loading curvature ratio E^*/C can be expressed as:

$$\frac{E^*}{C} = \frac{1}{f_1\left(\frac{Y}{E^*}, n\right)} = f_2\left(\frac{E^*}{Y}, n\right) \tag{9}$$

For a given conical/pyramid indenter, the indentation unloading force P_u can be expressed as (Dao et al., 2001):

$$P_u = P_u(h, h_m, E^*, Y, n) \tag{10}$$

The initial slop at unloading is thus determined by:

$$\left.\frac{\mathrm{d}P_u}{\mathrm{d}h}\right|_{h=h_m} = \left.\frac{\mathrm{d}P_u}{\mathrm{d}h}(h, h_m, E^*, Y, n)\right|_{h=h_m} \tag{11}$$

According to dimensional analysis, the initial slop at unloading is obtained:

$$\left.\frac{\mathrm{d}P_u}{\mathrm{d}h}\right|_{h=h_m} = E^* h_m f_3\left(\frac{h_m}{h_m}, \frac{E^*}{Y}, n\right) \tag{12}$$

Eq. (12) is then rearranged as

$$\frac{S}{E^* h_m} = f_4\left(\frac{E^*}{Y}, n\right) \tag{13}$$

Combining Eqs. (9) and (13) leads to

$$\frac{S}{C h_m} = f_5\left(\frac{E^*}{Y}, n\right) \tag{14}$$

Further, Cheng et al. (2002) have derived the following equations:

$$\frac{W_p}{W_t} = f_w(Y, E, n, \nu, \theta) \tag{15a}$$

$$\frac{h_r}{h_m} = f_h(Y, E, n, \nu, \theta) \tag{15b}$$

Hence, for a given conical/pyramid indenter Eqs. (15) can be written as below:

$$\frac{W_p}{W_t} = f_6\left(\frac{E^*}{Y}, n\right) \tag{16a}$$

$$\frac{h_r}{h_m} = f_7\left(\frac{E^*}{Y}, n\right) \tag{16b}$$

2.2. Finite element model

Since the indentation problem of a rigid cone into half-space is axisymmetric (Fig. 1a) only one-half of the system is used in the modeling. Therefore, elastic–plastic indentation was simulated using the axisymmetric capacities of the MARC/MSC finite element code. The conical indenters of half included angles of 70.3°

Table 1
FEA and forward results for Al 6061 and Al 7075 aluminums

	$C_{70.3}$ (GPa)	$(S/(Ch_m))_{70.3}$	$(W_p/W_t)_{70.3}$	C_{60} (GPa)
(a) *Al 6061-T6511*				
Experiments (Dao et al., 2001; Chollacoop et al., 2003)	27.4	16.4455	0.896	11.27
FEA results	26.9	16.7731	0.8979	11.1873
Deviation (%)	−1.81	1.99	0.21	−0.73
Forward results		16.6461	0.9030	11.37
Deviation (%)		1.22	0.78	0.93
(b) *Al 7075-T651*				
Experiments (Dao et al., 2001; Chollacoop et al., 2003)	41.2	10.2256	0.833	17.60
FEA results	42.8892	10.1343	0.8350	18.90
Deviation (%)	4.10	−0.89	0.25	7.39
Forward results		10.7193	0.8501	18.17
Deviation (%)		4.83	2.05	3.24

All deviations were computed as $\frac{X_{\text{calculation}}-X_{\text{experiment}}}{X_{\text{experiment}}}$, where X represents a variable.

and 60° were modeled as rigid bodies. The first indenter ($\theta_1 = 70.3°$) corresponds to commonly used Berkovich and Vickers indenters. The second indenter ($\theta_2 = 60°$) was chosen, because it would not produce significant friction effects to the indentation results according to Bucaille et al. (2003) and a large difference between half included angles of dual indenters, $(\theta_1 - \theta_2)$, improves identified results (Cao and Lu, 2004) as well as reduces almost wholly the range of mystical materials (Chen et al., 2007).

Since any typical indentation experiment would involve blunting of the indenter tip, the cone tip was smoothed by a sphere of radius much smaller than the indentation depth. This also eliminates any possible convergence errors due to sharp corners. The specimen was modeled as a large cylinder represented by around 10,100 large strain four-node axisymmetric elements. The radius and the height of the sample are equal or forty times larger than the contact radius. These dimensions were found to be large enough to approximate a semi-infinite half-space for indentations. This was evidenced by an insensitivity of calculated results to further increase in specimen size.

Elements were finest in the central contact area and became gradually coarser outwards. At the maximum indentation depth $h_m = 5$ μm, no less than 30 elements came into contact. It enables an accurate determination of the real impression size. Frictionless roller boundary conditions were applied along the centerline and bottom. Outside surfaces were taken as free surfaces. The interaction between the rigid indenter and the specimen was modeled by contact elements without friction. Residual stresses were not taken into account in the analysis. Displacement-controlled procedure was used in this work.

A large number of modeled materials with n ranging from 0 to 0.5 and Y/E ranging from 0.003 to 0.04 were used in the computations. Their mechanical properties are detailed in Table A1 in the appendix. The finite element model was well tested for convergence and accuracy, and then validated by comparing the indentation parameters obtained by FEA with experimental data for Al 6061-T6511 and Al 7075-T651 aluminum alloys reported by Dao et al. (2001) and Chollacoop et al. (2003), see Table 1 in Section 5.1. Further, FEA results are compared with the modeling results obtained by Dao et al. (2001), Cheng et al. (2002), and Tho et al. (2005) (see Fig. 2). This also proves the validity of the finite element model.

3. Independent relationships for a single indentation load–depth curve

3.1. Relationship between W_p/W_t (or W_t/W_e) and h_r/h_m (or h_m/h_e)

Lawn and Howes (1981) have first explored a non-linear correlation between W_p/W_t and h_r/h_m by studying the elastic recovery of several ceramic materials and steels. Recently, by using dimensional analysis and finite element calculations, Cheng et al. (2002) established a one-to-one correspondence between W_p/W_t and h_r/h_m, and showed that this dimensionless relationship is independent of mechanical properties as well as of half

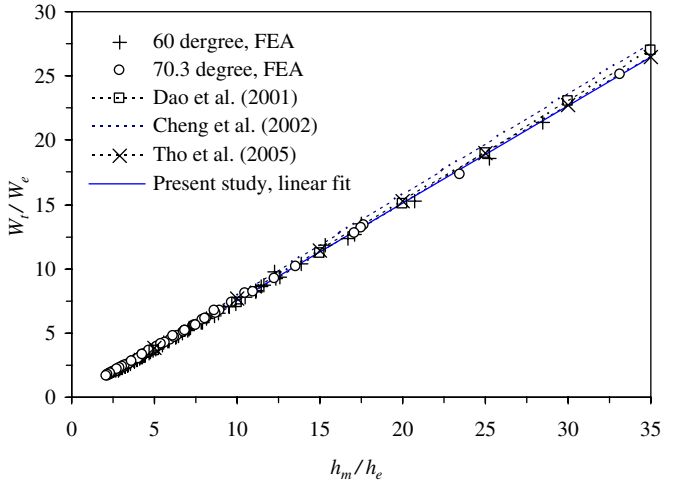

Fig. 2. Relationship between W_t/W_e and h_m/h_e.

included angles ranging from 45° to 80°. Furthermore, this relationship is approximately linear for $h_r/h_m > 0.4$ or for $W_p/W_t > 0.2$ as follows:

$$\frac{W_p}{W_t} = 1.27\frac{h_r}{h_m} - 0.27 \tag{17}$$

Subsequently, Dao et al. (2001) proposed a non-linear equation relating these two quantities for $\theta = 70.3°$. Tho et al. (2005) proposed a linear relationship between W_p/W_t and h_m/h_e (where $h_e = h_m - h_r$) for the indenter of $\theta = 70.3°$ as follows:

$$\frac{W_p}{W_t} = -1.2973\frac{h_e}{h_m} - 0.9993 \tag{18}$$

Considering Eqs. (3) and (4), a relation between W_t/W_e and h_m/h_e can be derived as

$$\frac{W_t}{W_e} = \frac{m+1}{3}\frac{h_m}{h_e} \tag{19}$$

It is noted that

$$\frac{W_t}{W_e} = \frac{1}{1-\frac{W_p}{W_t}} \tag{20a}$$

and

$$\frac{h_m}{h_e} = \frac{1}{1-\frac{h_r}{h_m}} \tag{20b}$$

The evolution of W_t/W_e versus h_m/h_e is plotted in Fig. 2. It is noted that $h_r/h_m > 0.5$ (thus $h_m/h_e > 2$) for all modeled materials. The exponent of the unloading curve, m, has been discussed in Oliver and Pharr (1992), Marx and Balke (1997) and Pharr and Bolshakov (2002). It varies from 1.2 to 1.6 for common metals and engineering alloys in Berkovich or equivalent conical indentation tests (Pharr and Bolshakov, 2002) and depends on the indented material's mechanical properties. It is shown in Fig. 2 that an approximate linear law can be found with a fitted value of $m = 1.32$. The equations suggested by Cheng et al. (2002) and Tho et al. (2005) with considering $0.9993 \approx 1$ can be derived from Eqs. (19) when taking m as 1.3622 and 1.3125, respectively. Variations of W_t/W_e versus h_m/h_e according to equations proposed by Dao et al. (2001), Cheng et al. (2002), and Tho et al. (2005) are also included in Fig. 2 for comparison purpose.

3.2. Relationship between $S/(Ch_m)$ and h_m/h_e

To evaluate the initial unloading slope S, the 67% upper unloading curve is used to obtain a similar power law equation as Eq. (4):

$$P_u = A_1(h - h_r)^{m_1}. \tag{21}$$

It is remarked that $m_1 < m$ since less used data in Eq. (21) than in Eq. (4) (Marx and Balke, 1997). A relation between $S/(Ch_m)$ and h_m/h_e can be found from Eqs. (3) and (4) as follows:

$$\frac{S}{Ch_m} = m_1 \frac{h_m}{h_e} \tag{22}$$

The evolution of $S/(Ch_m)$ versus h_m/h_e is depicted in Fig. 3. A linear law can be derived by a least square fitting procedure with a fitted value of $m_1 = 1.2$.

3.3. Relationship between $S/(Ch_m)$ and W_t/W_e

From Eqs. (19) and (22), a relation between $S/(Ch_m)$ and W_t/W_e can be written under the following form:

$$\frac{S}{Ch_m} = \frac{3m_1}{m+1} \frac{W_t}{W_e} \tag{23}$$

Fig. 4 shows the variation of $S/(Ch_m)$ versus W_t/W_e. A linear law can be derived for all data with $m = 1.27$ and $m_1 = 1.2$. It should be emphasized that for rigid-perfectly-plastic materials, $m = m_1 = 1$, and S, W_t/W_e and $h_m/h_e \to \infty$. For elastic materials, $m = m_1 = 2$ and, $S/(Ch_m) = 2$, $W_t/W_e = h_m/h_e = 1$. Thus, Eqs. (19), (22), and (23) are also validated in these two limit cases.

It is indicated that it exits one-to-one correspondent relationships between one and other from three dimensionless indentation parameters $S/(Ch_m)$, W_t/W_e, and h_m/h_e. These relationships are independent of mechanical properties as well as of indenter apex angle. Consequently, only two of four indentation parameters of a single indentation load-depth curve, S, C, W_t/W_e, and h_m/h_e, are independent, leading to two independent equations, which contain the information on the indented material's mechanical properties. Despite this, three independent equations are required in the reverse analysis to estimate three mechanical properties E^*, Y, n. These results support the reason for non-unique reverse solution based on load–displacement curves of a single indenter (Cheng and Cheng, 1999; Capehart and Cheng, 2003; Alkorta et al., 2005; Tho et al., 2005; Luo et al., 2006).

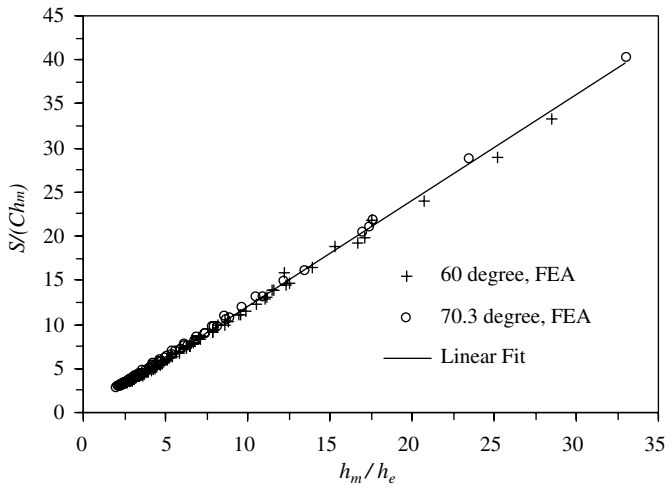

Fig. 3. Relationship between $S/(Ch_m)$ and h_m/h_e.

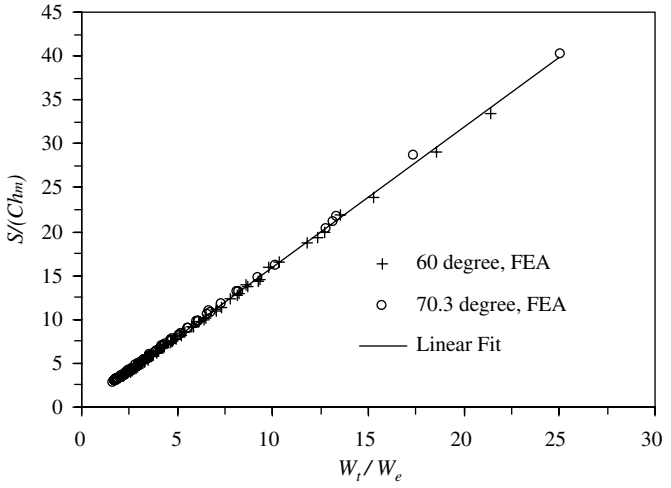

Fig. 4. Relationship between $S/(Ch_m)$ and W_t/W_e.

4. Dependent relationships

4.1. Dimensionless relationships for $S/(Ch_m)$, W_t/W_e, and h_m/h_e as functions of E^*/C and n

Combining Eqs. (16) and (20) leads to

$$\frac{W_t}{W_e} = f_8\left(\frac{E^*}{Y}, n\right) \tag{24}$$

$$\frac{h_m}{h_e} = f_9\left(\frac{E^*}{Y}, n\right) \tag{25}$$

It is noted that whenever n and E^*/C are known, E^*/Y can be determined according to Eqs. (9). Therefore, regarding Eqs. (9), (14), (24) and (25), E^*/C can be used instead of E^*/Y to express the indentation parameters such as:

$$\frac{S}{Ch_m} = f_{10}\left(\frac{E^*}{C}, n\right) \tag{26a}$$

$$\frac{W_t}{W_e} = f_{11}\left(\frac{E^*}{C}, n\right) \tag{26b}$$

$$\frac{h_m}{h_e} = f_{12}\left(\frac{E^*}{C}, n\right) \tag{26c}$$

The evolutions of $S/(Ch_m)$, W_t/W_e, and h_m/h_e as function of E^*/C and n are shown in Fig. 5. At a given value of n, the dimensionless parameters $S/(Ch_m)$, W_t/W_e, and h_m/h_e increase linearly with E^*/C (the correlation coefficient, $R^2 \geqslant 0.9995$ in all studied cases). Eqs. (26) can be expressed as follows:

$$\frac{S}{Ch_m} = K_{sc1}(n)\frac{E^*}{C} + K_{sc2}(n) \tag{27a}$$

$$\frac{W_t}{W_e} = K_{w1}(n)\frac{E^*}{C} + K_{w2}(n) \tag{27b}$$

$$\frac{h_m}{h_e} = K_{h1}(n)\frac{E^*}{C} + K_{h2}(n) \tag{27c}$$

where K_{ns1}, K_{ns2}, K_{nw1}, K_{nw2}, K_{nh1} and K_{nh2}, are detailed in the Appendix.

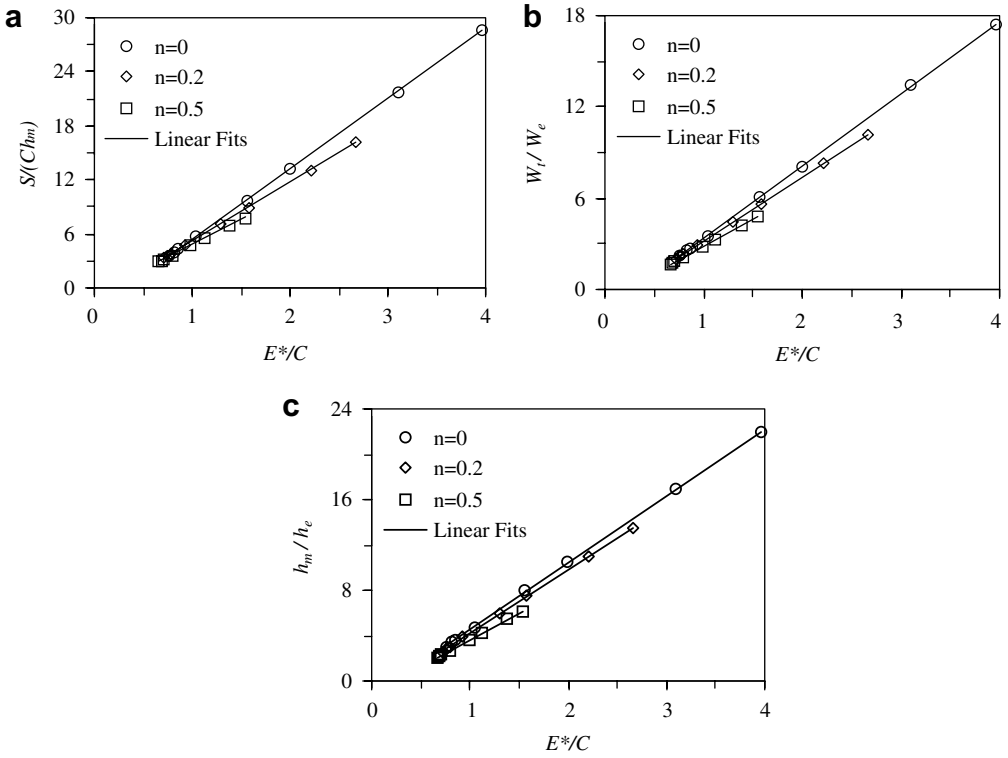

Fig. 5. Relationship between: (a) $S/(Ch_m)$, (b) W_t/W_e and (c) h_m/h_e versus E^*/C for $\theta = 70.3°$.

4.2. Relationships between corresponding parameters with dual indenters

By conducting a similar dimensional analysis as in the previous section, it is found that instead of E^*/Y, $E^*/C_{70.3}$ can be used to govern the evolution of E^*/C_{60}. Fig. 6 shows linear relationships between E^*/C_{60} and $E^*/C_{70.3}$ for different values of n (the correlation coefficient, $R^2 \geqslant 0.9996$ in all studied cases). General relation between E^*/C_{60}, $E^*/C_{70.3}$ and n can be written as below

$$\frac{E^*}{C_{60}} = D_{ec1}(n)\frac{E^*}{C_{70.3}} + D_{ec2}(n) \tag{28}$$

where $D_{ec1}(n)$ and $D_{ec2}(n)$ are given in the Appendix.

From Eqs. (27) and (28), linear relationships between corresponding dimensionless parameters can be derived for dual indenters as follows:

$$\left(\frac{S}{Ch_m}\right)_{60} = D_{sc1}(n)\left(\frac{S}{Ch_m}\right)_{70.3} + D_{sc2}(n) \tag{29a}$$

$$\left(\frac{W_t}{W_e}\right)_{60} = D_{w1}(n)\left(\frac{W_t}{W_e}\right)_{70.3} + D_{w2}(n) \tag{29b}$$

$$\left(\frac{h_m}{h_e}\right)_{60} = D_{h1}(n)\left(\frac{h_m}{h_e}\right)_{70.3} + D_{h2}(n) \tag{29c}$$

These linear variations are shown in Fig. 7 (the correlation coefficient, $R^2 \geqslant 0.9995$ in all studied cases). The coefficients of Eqs. (29) are detailed in the appendix. It should be emphasized that only one mechanical property (the strain hardening exponent, n) is involved in Eqs. (29). Hence, n can be easily estimated from these relations in the reverse analysis.

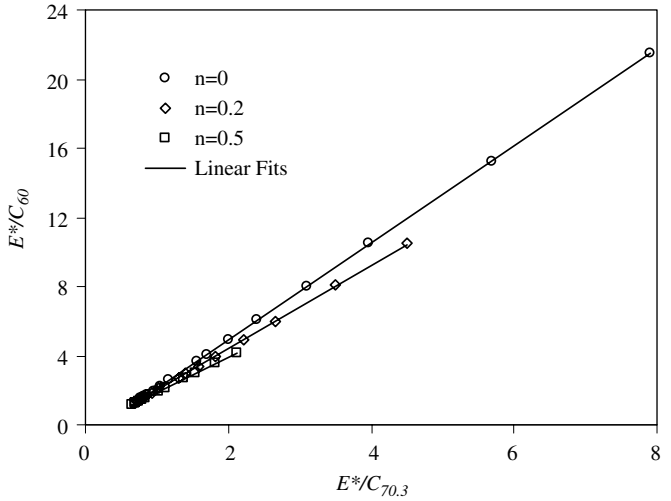

Fig. 6. Relationship between E^*/C_{60} and $E^*/C_{70.3}$.

5. Forward, reverse and sensitivity analysis

5.1. Forward analysis

It is remarked here that the yield strength Y is absent in the above formulated relations since the indentation parameters are expressed as functions of E^*/C and n, therefore the forward analysis scheme enables to predict the indentation force–displacement response of a material when knowing E^*, n, and the loading curvature associated to one indenter $C_{70.3}$ (or C_{60}). The loading curvature C is supposed to be known by mean of experiment or FEA. In the forward analysis, C_{60} (or $C_{70.3}$) is estimated by using Eq. (28), then other indentation parameters such as S, W_t/W_e, h_m/h_e for two indenters $\theta = 60°$ and $\theta = 70.3°$ are evaluated according to Eqs. (27) and (29).

The forward analysis was first conducted for two aluminum alloys which were previously investigated by Dao et al. (2001) and Chollacoop et al. (2003). Table 1 lists the principal indentation parameters which are the average values from different indentation tests. It is noted that $S/(Ch_m)$ can be calculated from experimental values of S and C, and the maximum indentation depth h_m, which is evaluated by using Eq. (4) when knowing the maximum indentation force. Further details in mechanical properties and instrumented indentation tests of these two aluminum alloys are available in the literature (Dao et al., 2001; Chollacoop et al., 2003). After obtaining W_t/W_e from Eq. (27b), W_p/W_t is calculated by using Eqs. (20a).

The FEA results and the forward analysis results for these two aluminum alloys are also shown in Table 1. A good agreement between calculated results and experimental data is achieved especially for Al 6061-T6511 aluminum alloy. Deviation between calculations (FEA and forward analysis) and experimental results for the loading curvature C is slightly high in the case of Al 7075-T651 aluminum alloy due to a large scatter in experimental data (Chollacoop et al., 2003).

Ten representative materials were chosen for the forward analysis in the next step. Their mechanical properties are listed in Table 2. The Poisson's ratio is taken as 0.3. The first eight materials in Table 2 correspond to usual metals and engineering alloys which have been investigated as representative materials in previous works (Bucaille et al., 2003; Swaddiwudhipong et al., 2005; Luo and Lin, 2007). The last two materials are a rare pair of mystical materials for the dual indenters ($\theta_1 = 70.3°$ and $\theta_2 = 60°$) according to Chen et al. (2007). These two special materials are further discussed in the next sections.

Due to the length of the paper, forward analysis was carried out only for $(W_t/W_e)_{70.3}$ and $(W_t/W_e)_{60}$ by using Eqs. (27b) and (29b). Table 3 shows a good agreement between FEA results and forward analysis results for representative materials.

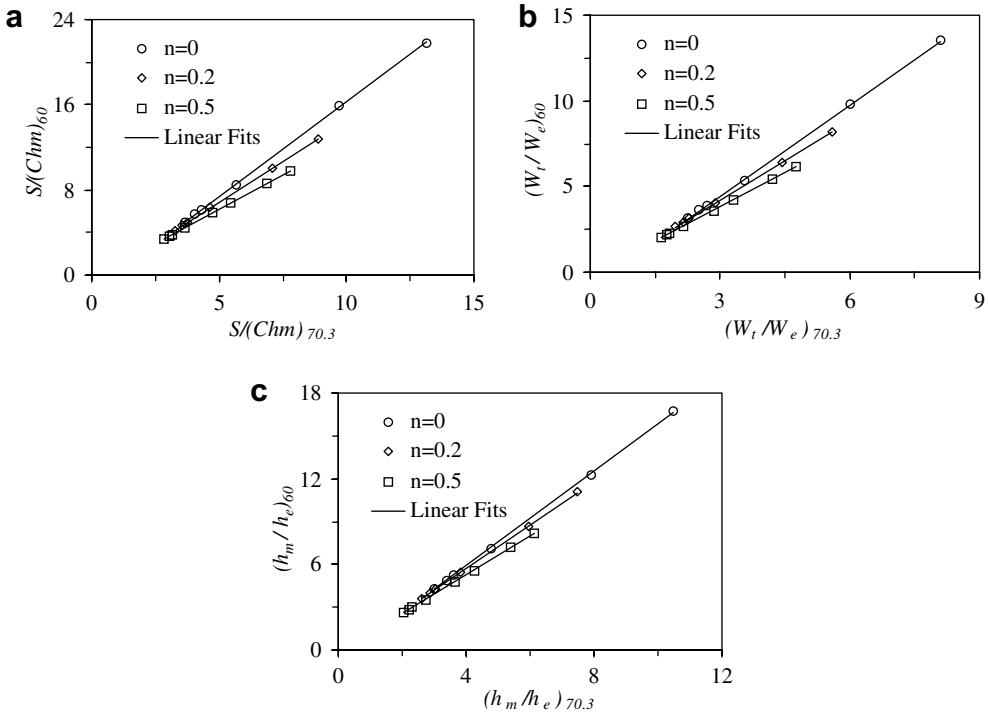

Fig. 7. Relationships between corresponding parameters with dual indenters: (a) $S/(Ch_m)_{60}$ and $S/(Ch_m)_{70.3}$, (b) $(W_t/W_e)_{60}$ and $(W_t/W_e)_{70.3}$, and (c) $(h_m/h_e)_{60}$ and $(h_m/h_e)_{70.3}$.

5.2. Reverse analysis

In practice, it is difficult to evaluate accurately h_m/h_e. Hence, W_p/W_t (or W_t/W_e), S, and C are employed in the reverse analysis. Based on the formulated equations, several possibilities may be considered to solve the reverse problem.

Experimental data on two aluminum alloys investigated by Dao et al. (2001) and Chollacoop et al. (2003) are utilized in the present work to verify the reverse analysis procedure.

Dao et al. (2001) reported that the plastic indentation work-total indentation work ratio W_p/W_t can be estimated in practice more accurately than the loading curvature C and the initial unloading slope S. Obviously, it may be imagined that uncertainties of W_p/W_t and W_t/W_e are less than those of other indentation parameters because all data of entire loading and unloading indentation P–h curves are exploited. Unfortunately, experimental results of W_t/W_e for these two aluminum alloys were not reported in Dao et al. (2001) and Chollacoop et al. (2003). It is evident that W_t/W_e can be evaluated from experimental values of W_p/W_t by using Eq. (20a). However with typical $\pm 1\%$ error in W_p/W_t as remarked in Dao et al. (2001) and Chollacoop et al. (2003), calculated values of W_t/W_e can rise to $\pm 10\%$ errors for these two materials.

Therefore, experimental data of $(S/(Ch_m))_{70.3}$, $C_{70.3}$, and C_{60} are utilized in the reverse analysis for these two aluminum alloys. In the remainder of the paper, $(W_t/W_e)_{60}$, $(W_t/W_e)_{70.3}$, and $C_{70.3}$ are used in the reverse analysis for modeled materials.

In the reverse analysis, Eqs. (27a) and (28) are solved to evaluate E^* and n for two aluminum alloys with the use of $(S/(Ch_m))_{70.3}$, $C_{70.3}$, and C_{60} as input data. The estimated mechanical properties of these two aluminum are tabulated in Table 4, showing good inverse results for Al 6061-T6511 aluminum alloy. Although the strain hardening exponent is considerably underestimated for Al 7075-T651 aluminum alloy due to a large scatter in experimental data of $C_{70.3}$ and C_{60} (Chollacoop et al., 2003), the error in reduced elastic modulus is still acceptable in practice (-7.66%).

Table 2
Mechanical properties of the representative materials

Materials	E (GPa)	Y (MPa)	n
Aluminum (Al)	70	500	0.122
Copper (Cu)	128	10	0.5
Iron	180	300	0.25
Nickel (Ni)	207	800	0.4
Steel 1 (S1)	210	500	0.1
Steel 2 (S2)	210	900	0.3
Titanium (Ti)	110	600	0.1
Zinc (Zn)	9	300	0.05
Material 9 (M9)	100	872.47	0
Material 10 (M10)	103.75	715.61	0.10663

Table 3
FEA and forward results for representative materials

Materials	$C_{70.3}$ (GPa) FEA	$(W_t/W_e)_{70.3}$ FEA	$(W_t/W_e)_{70.3}$ Eq. (27b)	% Error $(W_t/W_e)_{70.3}$	$(W_t/W_e)_{60}$ FEA	$(W_t/W_e)_{60}$ Eq. (29b)	% Error $(W_t/W_e)_{60}$
Aluminum	44.965	6.3526	6.3580	0.08	9.6982	9.7844	0.89
Copper	17.981	26.2746	26.6372	1.38	34.7702	35.0777	0.88
Iron	56.048	13.3886	13.3891	0.00	19.8055	19.6529	−0.77
Nickel	139.382	5.3318	5.3002	−0.59	7.1984	7.0944	−1.44
Steel 1	60.025	15.9063	15.9144	0.06	25.8296	25.6022	−0.88
Steel 2	127.279	6.2877	6.2654	−0.35	8.8941	8.8046	−1.01
Titanium	57.630	8.1510	8.1416	−0.12	12.7845	12.8284	0.34
Zinc	12.282	2.4215	2.4139	−0.31	3.4334	3.4339	0.02
Material 9	64.334	6.6979	6.6975	−0.01	11.0115	11.0185	0.06
Material 10	64.068	6.6775	6.7067	0.44	10.3578	10.4336	0.73

All deviations were computed as $\frac{X_{\text{prediction}}-X_{\text{FEA}}}{X_{\text{FEA}}}$, where X represents a variable.

In the next step, FEA results of 88 modeled materials (see Table A1 in the appendix) were used as input to verify the reversibility of the reverse analysis procedure. Eqs. (29b) is first solved to obtain the strain hardening exponent n, then the reduced elastic modulus E^* is evaluated by using Eq. (27b). Deviations in the strain hardening exponent n vary from -0.05 to 0.07. Errors in the reduced elastic modulus E^* appear within $\pm 1.7\%$.

Finally, reverse analysis was conducted for 10 representative materials. The indentation P–h curves of each material with respect to the dual indenters were obtained by FEA using the known material properties. These numerically generated indentation loading and unloading curves are used as input to the reverse analysis process in order to extract the mechanical properties of representative materials.

Table 5 shows in general good reverse results compared with original data, even for the extreme case of copper with a very low value of Y/E and high strain hardening. It should be emphasized that copper, iron and steel 1 exhibit their Y/E ratios falling well out side the range of modeled materials ($0.003 \leqslant Y/E \leqslant 0.04$), which were used to establish dimensionless functions in the present work. However, the linearity of formulated relationships apportions a great advantage when working in a wide range of materials.

Reverse analysis results are also very good for the last two special materials. They yield almost identical P–h curves for the first indenter with $\theta_1 = 70.3°$ as seen in Fig. 8. Their corresponding indentation parameters are accordingly very close in this case as shown in Table 6. Deviations in corresponding parameters appear within 3% in this case.

For the second indenter with $\theta_2 = 60°$, their P–h curves are fairly distinguishable. It is highlighted that deviations in their plastic indentation work-total indentation work ratios W_p/W_t fall within 1% for both two indenters. Thus, any reverse analysis based on W_p/W_t would fail for these two materials. Significant deviations in $S/(Ch_m)$ and W_t/W_e are found for the second indenter ($\theta_2 = 60°$). Consequently, reserve analysis based on these two parameters may be possible as the present study.

5.3. Sensitivity analysis

Sensitivity of the reverse solution to variations of input data with dual indenters has been previously investigated by several research works (Bucaille et al., 2003; Chollacoop et al., 2003; Cao and Lu, 2004; Swaddiwudhipong et al., 2005; Lan and Venkatesh, 2007). Bucaille et al. (2003) have shown that an increase of 3% in the loading curvature C leads to a difference of 44% on the value of n for steel. Swaddiwudhipong et al. (2005) reported that due to $\pm 2\%$ errors in C_{60} and $C_{70.3}$, and $\pm 1\%$ errors in $(W_p/W_t)_{60}$ and $(W_p/W_t)_{70.3}$, the maximum variation of E^* is close to 20% for low strain hardening materials, the maximum variation of Y can reach approximately 70% for high strain hardening materials and 30% with $n < 0.4$, the maximum variation of n ranges from 0.05 to 0.1 for a large value of n. The strain hardening exponent, n, is obtained with moderate sensitivity even though multiple indenters have been used in the reverse analysis (Bucaille et al., 2003; Chollacoop et al., 2003; Lan and Venkatesh, 2007).

Four cases of perturbations of the input data are considered in this work (see Table 7). Sensitivity analysis was carried out for 10 representative materials. Maximum deviations in absolute values in each case are depicted in Figs. 9 and 10 for the strain hardening exponent and the reduced elastic modulus, respectively.

It should be emphasized that estimated values of n depend only on $(W_t/W_e)_{60}$ and $(W_t/W_e)_{70.3}$. Predicted values of E^* depend on $(W_t/W_e)_{70.3}$, $C_{70.3}$, and n. In general, due to variations of the input data, deviation of n is less than 0.07 in cases 1 and 2, and less than 0.11 in the last two cases.

Excepting that zinc is an extreme case with a high value of Y/E and a very low strain hardening. Without any perturbation of the input data, the strain hardening exponent of zinc was unsuccessfully determined by several previous methods. This exponent was estimated as 0.1 by Dao's method (Dao et al., 2001) according to Bucaille et al. (2003), as 0 for other methods with dual indenters (Bucaille et al., 2003; Swaddiwudhipong

Table 4
Reverse analysis results for Al 6061 and Al 7075 aluminum alloys

	E^* (GPa)	% Error E^*	n
(a) Al 6061-T6511			
Tensile tests	70.2		0.08
Present study	68.7	−2.14	0.0613
Chollacoop et al. (2003)	70.1	−0.14	
(b) Al 7075-T651			
Tensile tests	73.4		0.122
Present study	67.78	−7.66	0.0334
Chollacoop et al. (2003)	79.3	8.04	

All deviations were computed as $\frac{X_{\text{prediction}} - X_{\text{experiment}}}{X_{\text{experiment}}}$, where X represents a variable.

Table 5
Reverse analysis results for representative materials

Materials	Original data		Reverse analysis			
	E (GPa)	n	E (GPa)	% Error E	n	Deviation of n
Aluminum	70	0.122	70.36	0.51	0.1372	0.015
Copper	128	0.5	125.36	−2.07	0.4870	−0.013
Iron	180	0.25	179.99	0.00	0.2500	0.000
Nickel	207	0.4	206.27	−0.35	0.3786	−0.021
Steel 1	210	0.1	208.38	−0.77	0.0854	−0.015
Steel 2	210	0.3	209.47	−0.25	0.2865	−0.014
Titanium	110	0.1	110.49	0.44	0.1082	0.008
Zinc	9	0.05	9.06	0.69	0.0902	0.040
Material 9	100	0	100.05	0.05	0.0013	0.001
Material 10	103.75	0.10663	103.57	−0.18	0.1117	0.005

All deviations were computed as $\frac{X_{\text{prediction}} - X_{\text{original}}}{X_{\text{original}}}$, where X represents a variable.

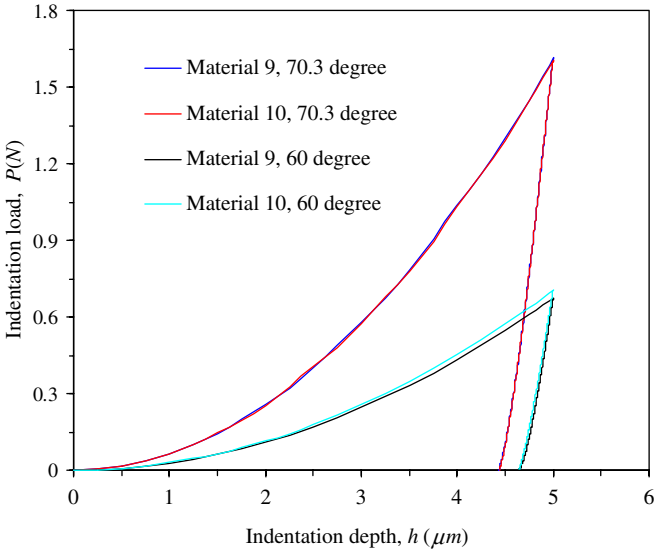

Fig. 8. Indentation load–depth curves of two special materials.

Table 6
Principal indentation parameters of the typical pair of mystical materials

	C (GPa)	S (N/mm)	$S/(Ch_m)$	W_p/W_t	W_t/W_e
$\theta_1 = 70.3°$					
Material 9	64.334	3523.1	10.9526	0.85070	6.6979
Material 10	64.068	3425.2	10.6923	0.85024	6.6775
Deviation (%)	−0.41	−2.78	−2.38	−0.05	−0.30
$\theta_2 = 60°$					
Material 9	26.987	2424.1	17.9651	0.90919	11.0115
Material 10	28.319	2305.7	16.2838	0.90345	10.3578
Deviation (%)	4.94	−4.88	−9.36	−0.63	−5.94

All deviations were computed as $\frac{X_{10}-X_9}{X_9}$, where X represents a variable.

et al., 2005). To obtain an acceptable result for zinc, it was necessary to use four indenters as reported by Bucaille et al. (2003). This material also exhibits high deviations in the strain hardening exponent, as 0.13 in cases 1 and 2, and 0.19 in cases 3 and 4.

Copper is another extreme material with exceptionally low value of Y/E and high strain hardening. It presents the highest sensitivity in estimated values of E^* (up to 7.6%, 9.5%, 11%, and 12.7% in cases 1, 2, 3 and 4, respectively). For other materials, errors in the reduced elastic modulus E^* are within ±5.3%, ±7.3%, ±9%, and ±11% in cases 1, 2, 3 and 4, respectively.

Other low strain hardening materials (aluminum, steel 1, titanium, materials 9 and 10) exhibit approximate deviations in the strain hardening exponent. These deviations vary within 0.04 in cases 1 and 2, and within 0.09 in cases 3 and 4.

Despite the moderate sensitivity of the strain hardening exponent, it is found that the reduced elastic modulus is much less sensitive and remains in practice acceptable when facing typical uncertainties of input data. Previous works have also found lower sensitivities in estimated elastic modulus than those in yield strength and in strain hardening exponent (Bucaille et al., 2003; Chollacoop et al., 2003; Cao and Lu, 2004; Swaddiwudhipong et al., 2005; Lan and Venkatesh, 2007).

Correlation between the sensitivity and the new concept *mystical materials* recently proposed by Chen et al. (2007) may be considered, even though their work has focused on the unique reverse solu-

Table 7
Case study for sensitive analysis of representative materials

Case study	Changes in the input data	
	% Error in $C_{70.3}$	% Error in $(W_t/W_e)_{70.3}$ and $(W_t/W_e)_{60}$
Case 1	±2	±1
Case 2	±4	±1
Case 3	±2	±2
Case 4	±4	±2

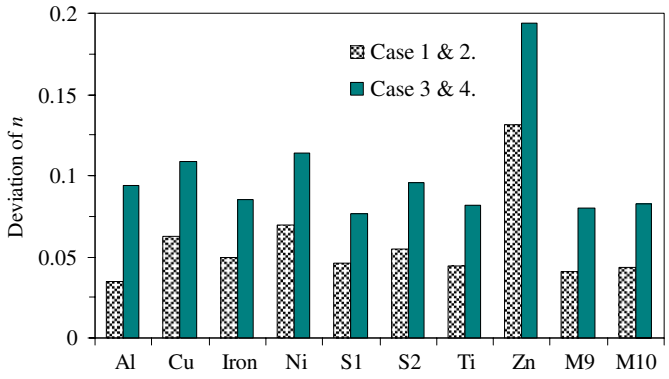

Fig. 9. Sensitivity study on the strain hardening exponent n.

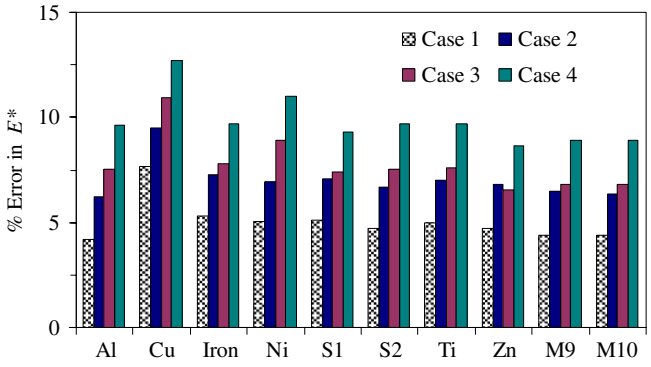

Fig. 10. Sensitivity study on the reduced elastic modulus E^*.

tion with dual sharp indenters rather than on the sensitivity. Regarding indentation responses with dual indenters of mystical materials (e.g., materials 9 and 10, see Table 6), which have been specified in Chen et al. (2007), it may be quantitatively understood that a pair of materials can be considered as *mystical materials* when most of their corresponding indentation parameters exhibit deviations being lower than 5%.

When a set of original indentation parameters of a tested material with dual indenters are perturbed by any mean, the resulted new one may probably match that of another material. These two materials may become candidates for a pair of mystical materials. It should be emphasized that such a pair of materials can fall well out side mystical materials maps indicated by Chen et al. (2007).

Following the procedure proposed by Chen et al. (2007) to search two candidates for a pair of mystical materials with dual indenters, it can be seen that candidate materials should exhibit *a priori* a lower deviation in elastic modulus than those in yield strength and in strain hardening exponent. It correlates to the fact that

the elastic modulus is less sensitive than other mechanical properties due to variations of input data as shown in the present study and in previous works (Bucaille et al., 2003; Chollacoop et al., 2003; Cao and Lu, 2004; Swaddiwudhipong et al., 2005; Lan and Venkatesh, 2007).

Although non-unique reverse solution can occur with certain dual indenters, the present work shows that by using the common dual indenters ($\theta_1 = 70.3°$ and $\theta_2 = 60°$), the elastic modulus and the strain hardening can be extracted at least for the range of considered materials (including a pair of mystical materials). It is severe to deal with mystical materials, which experience almost identical P–h curves for different indenters. However, it is interesting to point out that their elastic modulus can be accurately estimated even with certain perturbations of input data due to their characteristics: *fair difference in elastic modulus*.

6. Conclusions

In the present work, several fundamental issues in instrumented sharp indentations are investigated. The main results are summarized as follows:

- Concerning to the characteristics of P–h curves of a single indenter, there exit approximately linear relationships between one and other among three dimensionless indentation parameters: $S/(Ch_m)$, W_t/W_e, and h_m/h_e. These functional relations are independent of mechanical properties as well as of indenter apex angle. Hence, only two among four fundamental indentation parameters S, C, W_t/W_e, and h_m/h_e are independent. These results clearly demonstrate the non-unique reverse solution when using indentation load–displacement curves of a single indenter.
- A new approach is proposed to consider instrumented sharp indentation problems and to obtain simple functional forms. Although E^*/Y and n are the two key parameters governing the characteristics of load–displacement curves for elasto-plastic materials, the results show that E^*/C and n can be employed to express useful relationships for the characteristics of a single indenter. At a given strain hardening exponent, n, it is found that $S/(Ch_m)$, W_t/W_e and h_m/h_e increase almost linearly with E^*/C.
- The duality between corresponding dimensionless parameters is systematically studied for dual indenters. It is indicated that between two corresponding parameters (E^*/C_{60} and $E^*/C_{70.3}$, $S/(Ch_m)_{60}$ and $S/(Ch_m)_{70.3}$, $(W_t/W_e)_{60}$ and $(W_t/W_e)_{70.3}$, $(h_m/h_e)_{60}$ and $(h_m/h_e)_{70.3}$), there exist approximately linear relationships, in which only the strain hardening exponent is involved.
- The accuracy of the reverse procedure was verified with experimental data from the literature and representative materials. The reverse analysis shows in general good results, particularly for the reduced elastic modulus. In practice, uncertainties of input data are inevitable due to the friction between the indenter and the specimen, the imperfect indenter tip, etc. Therefore, considerable attention must be paid to the strain hardening exponent due to its moderate sensitivity. However, much less sensitivity was found for the elastic modulus and its predicted values remain still reasonable for a wide range of materials.

Acknowledgements

This work was partially supported by the Research Program of Hanoi University of Technology and the Basic Research Program from the Vietnamese Council for Science.

Appendix A

See Table A1.

The coefficients in Eqs. (27) for $\theta = 60°$:

Table A1
The material's mechanical properties used in the computations

E (GPa)	Y (MPa)	Y/E
10	30	0.003
50	200	0.004
130	910	0.007
10	100	0.01
50	1000	0.02
10	300	0.03
90	3000	0.0333
50	2000	0.04

Poisson's ratio, ν is fixed at 0.3. Strain hardening exponent, n, is taken as 0, 0.05, 0.1, 0.15, 0.2, 0.25, 0.3, 0.35, 0.4, 0.45, and 0.5, resulting a total of 88 different cases.

$$K_{sc1}(n) = 3.0478n^2 - 4.3481n + 4.9538;$$
$$K_{sc2}(n) = -4.1983n^2 + 5.36n - 2.3973;$$
$$K_{w1}(n) = 0.445n^2 - 1.7801n + 3.0479;$$
$$K_{w2}(n) = -0.781n^2 + 1.856n - 1.3683;$$
$$K_{h1}(n) = -1.629n^2 - 0.8804n + 3.9114;$$
$$K_{h2}(n) = 1.1081n^2 + 0.5211n - 1.5678;$$

and for $\theta = 70.3°$:

$$K_{sc1}(n) = 4.483n^2 - 6.752n + 7.7875;$$
$$K_{w1}(n) = 0.6432n^2 - 2.793n + 4.722;$$
$$K_{h1}(n) = -1.3413n^2 - 1.9426n + 6.0909.$$

It is noted that: $(K_{sc2})_{60} = (K_{sc2})_{70.3}$; $(K_{w2})_{60} = (K_{w2})_{70.3}$ and $(K_{h2})_{60} = (K_{h2})_{70.3}$. The coefficients in Eq. (28):

$$D_{ec1}(n) = -7.2075n^4 + 5.1015n^3 + 0.8993n^2 - 2.3107n + 2.8035;$$
$$D_{ec2}(n) = 13.8508n^4 - 12.9251n^3 + 1.9595n^2 + 1.5629n - 0.6898.$$

The coefficients in Eq. (29):

$$D_{sc1}(n) = -2.9397n^3 + 3.1879n^2 - 1.8119n + 1.7741;$$
$$D_{sc2}(n) = 12.3754n^3 - 13.3119n^2 + 5.8994n - 1.4616;$$
$$D_{w1}(n) = -0.5946n^3 + 1.3177n^2 - 1.41n + 1.7718;$$
$$D_{w2}(n) = 8.3408n^3 - 8.8549n^2 + 3.7705n - 0.8481;$$
$$D_{h1}(n) = 1.0502n^3 - 0.9974n^2 - 0.4001n + 1.6591;$$
$$D_{h2}(n) = -1.0709n^3 + 0.1876n^2 + 1.4022n - 0.728.$$

References

Alkorta, J., Martinez-Esnaola, J.M., Gil Sevillano, J., 2005. Absence of one-to-one correspondence between elastoplastic properties and sharp-indentation load-penetration data. J. Mater. Res. 20 (2), 432–437.

Atkins, A.G., Tabor, D., 1965. Plastic indentation in metals with cones. J. Mech. Phys. Solids 13, 149–164.

Bucaille, J.L., Stauss, S., Felder, E., Michler, J., 2003. Determination of plastic properties of metals by instrumented indentation using different sharp indenters. Acta Mater. 51, 1663–1678.

Cao, Y.P., Lu, J., 2004. Depth-sensing instrumented indentation with dual sharp indenters: stability analysis and corresponding regularization schemes. Acta Mater. 52, 1143–1153.

Capehart, T.W., Cheng, Y.T., 2003. Determining constitutive models from conical indentation: sensitivity analysis. J. Mater. Res. 18 (4), 827–832.

Chen, X., Ogasawara, N., Zhao, M., Chiba, N., 2007. On the uniqueness of measuring elastoplastic properties from indentation: the indistinguishable mystical materials. J. Mech. Phys. Solids 55, 1618–1660.

Cheng, Y.T., Cheng, C.M., 2004. Scaling, dimensional analysis, and indentation measurements. Mater. Sci. Eng. R Rep. 44 (4–5), 91–149.

Cheng, Y.T., Cheng, C.M., 1999. Can stress–strain relationships be obtained from indentation curves using conical and pyramidal indenters? J. Mater. Res. 14 (9), 3493–3496.

Cheng, Y.T., Li, Z., Cheng, C.M., 2002. Scaling relationships for indentation measurements. Philos. Mag. A 82 (10), 1821–1829.

Chollacoop, N., Dao, M., Suresh, S., 2003. Depth-sensing instrumented indentation with dual sharp indenters. Acta Mater. 51, 3713–3729.

Dao, M., Chollacoop, N., Van Vliet, K.J., Venkatesh, T.A., Suresh, S., 2001. Computational modeling of the forward and reverse problems in instrumented sharp indentation. Acta Mater. 49 (19), 3899–3918.

DiCarlo, A., Yang, H.T.Y., Chandrasekar, S., 2003. Semi-inverse method for predicting stress–strain relationship from cone indentations. J. Mater. Res. 18, 2068–2078.

Doerner, M.F., Nix, W.D., 1986. A method for interpreting the data from depth-sensing indentation instruments. J. Mater. Res. 1 (4), 601–609.

Fischer-Cripps, A.C., 2004. Nanoindentation. Springer-Verlag, New York.

Futakawa, M., Wakui, T., Tanabe, Y., Ioka, I., 2001. Identification of the constitutive equation by the indentation technique using plural indenters with different apex angles. J. Mater. Res. 16, 2283–2292.

Johnson, K.L., 1985. Contact Mechanics. Cambridge University Press.

Lan, H., Venkatesh, T.A., 2007. Determination of the elastic and plastic properties of materials through instrumented indentation with reduced sensitivity. Acta Mater. 55, 2025–2041.

Lawn, B.R., Howes, V.R., 1981. Elastic recovery at hardness indentations. J. Mater. Sci. (10), 2745–2752.

Lin, S., Hills, D.A., Warren, P.D., 2000. A theoretical investigation of sharp indentation testing of a nearly-brittle material, with some experimental results. J. Mech. Phys. Solids 48 (10), 2057–2075.

Luo, J., Lin, J., 2007. A study on the determination of plastic properties of metals by instrumented indentation using two sharp indenters. Int. J. Solids Struct. 44 (18–19), 5803–5817.

Luo, J., Lin, J., Dean, T.A., 2006. A study on the determination of mechanical properties of a power-law material by its indentation force–depth curve. Philos. Mag. 86 (19), 2881–2905.

Marx, V., Balke, H., 1997. A critical investigation of the unloading behavior of sharp indentation. Acta Mater. 45 (9), 3791–3800.

Ogasawara, N., Chiba, N., Chen, X., 2005. Representative strain of indentation analysis. J. Mater. Res. 20, 2225–2234.

Ogasawara, N., Chiba, N., Chen, X., 2006. Limit analysis-based approach to determine the material plastic properties with conical indentation. J. Mater. Res. 21, 947–958.

Oliver, W.C., Pharr, G.M., 1992. An improved technique for determining hardness and elastic-modulus using load and displacement sensing indentation experiments. J. Mater. Res. 7 (6), 1564–1583.

Oliver, W.C., Pharr, G.M., 2004. Review: measurement of hardness and elastic modulus by instrumented indentation: advances in understanding and refinements to methodology. Journal of Materials Research 19 (1), 3–20.

Pharr, G.M., Bolshakov, A., 2002. Understanding nanoindentation unloading curves. J. Mater. Res. 17 (10), 2660–2671.

Swaddiwudhipong, S., Tho, K.K., Liu, Z.S., Zeng, K., 2005. Material characterization based on dual indenters. Int. J. Solids Struct. 42, 69–83.

Tho, K.K., Swaddiwudhipong, S., Liu, Z.S., Zeng, K., 2005. Simulation of instrumented indentation and material characterization. Mater. Sci. Eng. A (1–2), 202–209.